Climate Dynamics manuscript No.
(will be inserted by the editor)

Mixed-phase clouds cause climate model biases in Arctic wintertime temperature inversions

Felix Pithan · Brian Medeiros · Thorsten Mauritsen

Received: date / Accepted: date

Abstract Temperature inversions are a common feature of the Arctic wintertime boundary layer. They have important impacts on both radiative and turbulent heat fluxes and partly determine local climate-change feedbacks. Understanding the spread in inversion strength modelled by current global climate models is therefore an important step in better understanding Arctic climate and its present and future changes. Here, we show how the formation of Arctic air masses leads to the emergence of a cloudy and a clear state of the Arctic winter boundary layer. In the cloudy state, cloud liquid water is present, little to no surface radiative cooling occurs and inversions are elevated and relatively weak, whereas surface radiative cooling leads to strong surface-based temperature inversions in the clear state. Comparing model output to observations, we find that most climate models lack a realistic representation of the cloudy state. An idealized single-column model experiment of the formation of Arctic air reveals that this bias is linked to inadequate mixed-phase cloud microphysics, whereas turbulent and conductive heat fluxes control the strength of inversions within the clear state.

Keywords Arctic · boundary layer · turbulence · temperature inversion

Felix Pithan
Max-Planck-Institute for Meteorology, Bundesstrasse 53, D-20146 Hamburg, Germany and
International Max Planck Research School on Earth System Modelling, Hamburg, Germany
E-mail: felix.pithan@mpimet.mpg.de

Brian Medeiros
National Center for Atmospheric Research, Boulder, USA

Thorsten Mauritsen
Max-Planck-Institute for Meteorology, Hamburg, Germany

1 Introduction

With temperatures rising faster than the global mean, a fast retreat in summertime sea-ice cover and increasing mass loss of glaciers and ice sheets, the Arctic climate system is undergoing profound changes (ACIA, 2004). Arctic processes have important implications for global climate through the formation of deep waters that sustain the oceanic meridional overturning circulation (e.g. Jungclaus et al, 2005), atmospheric connections to mid-latitude weather and climate (e.g. Honda et al, 2009; Francis and Vavrus, 2012) and climate feedbacks possibly relevant on the global scale. Understanding Arctic climate and climate change therefore remains an important challenge.

This paper aims to better understand Arctic temperature inversions and their representation in climate models. We combine CMIP5 model output and observational data with an idealised single-column model (SCM) experiment of the formation of Arctic air masses to investigate the processes that lead to the emergence and decay of temperature inversions. We find that low-level mixed-phase clouds play a key role in setting the surface fluxes and inversion strength, and many models struggle to represent these clouds at low temperatures.

Temperature inversions have important implications for the amplitude and sign of radiative and turbulent surface heat fluxes (Bintanja et al, 2011) as well as the mechanical coupling between surface and atmosphere and thus sea-ice drift (Overland and Guest, 1991). When the climate warms, the stable stratification of the atmosphere in the presence of temperature inversions acts to trap additional heat near the surface and thus contributes to a stronger warming near the surface than in the upper troposphere (Manabe and Wetherald, 1975). This vertical structure of Arctic warming causes a regionally positive lapse-rate feedback, because less warming in the upper troposphere leads to a smaller increase in

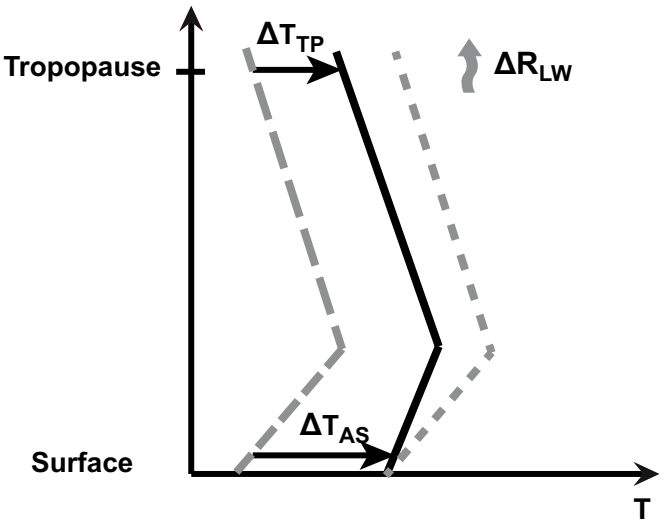

Fig. 1 Stronger warming at the surface than in the middle and upper troposphere leads to a positive lapse-rate feedback in the Arctic. Figure: Pithan and Mauritsen (2013) ©Americal Meteorological Society

outgoing longwave radiation compared to a vertically uniform warming. A smaller increase in outgoing radiation means that more surface warming is required to balance TOA fluxes and reach a steady state (Figure 1, see also Held, 1978).

Temperature inversions have been reported to be a typical feature of the Arctic atmosphere since some of the earliest scientific explorations of the Arctic (Sverdrup, 1933). Analysing radiosonde data from land-based and drifting stations, Serreze et al (1992) found that the frequency, depth and strength of wintertime temperature inversions increased from the Norwegian Sea to the east, where cloud cover is reduced and anticyclonic conditions become dominant. Temperature inversions were present in almost all soundings taken over one year for the Surface Heat Budget of the Arctic experiment (SHEBA) in pack ice north of Alaska (Tjernström and Graversen, 2009), with more than half of the observed inversions being surface-based in winter (DJF), while elevated inversions with a near-neutral mixed layer close to the surface dominated in spring and summer. Inversion strengths retrieved from satellite observations compare favourably with radiosonde stations at southern high latitudes and have also been used to extend our picture of Arctic temperature inversions (Gettelman et al, 2006; Pavelsky et al, 2011). Humidity inversions, i.e. specific humidity rising with altitude, are also common in Arctic boundary layers (Curry, 1986; Devasthale et al, 2011).

Interactions between radiation and cloud condensate play an important role for boundary layer development and inversion strength, as was already noted by Sverdrup (1933). Observations from the SHEBA campaign (Persson et al, 2002) revealed two preferred states of the Arctic wintertime boundary layer: A radiatively clear state characterised by strong longwave cooling under ice clouds or clear skies and a cloudy state with low-level mixed-phase clouds and little to no longwave cooling at the surface (Persson et al, 1999; Stramler et al, 2011). These states display distinct turbulent and conductive heat fluxes as well as vertical temperature structures with stronger, surface-based inversions occurring in the clear state and weaker, usually elevated inversions in the cloudy state (Figure 2).

Arctic stratiform mixed-phase clouds typically consist of one or several thin layers of supercooled liquid water at cloud top, with ice crystals within and below the liquid layer (Morrison et al, 2012). Liquid water is mostly formed in updrafts and to a minor extent in the inversion layer, while ice crystals are formed within the cloud, grow and are removed by sedimentation. The presence of ice can lead to a rapid depletion of cloud liquid water via the Wegener-Bergeron-Findeisen process (Wegener, 1911; Bergeron, 1935; Findeisen, 1938), and it has been suggested that low in-cloud concentrations of ice nuclei limit ice formation and thus contribute to the persistence of Arctic mixed-phase clouds (Fridlind et al, 2012). Turbulent updrafts and their effect on cloud processes cannot be resolved in large scale models and thus need to be parameterized. Most climate models also have too coarse a vertical resolution to resolve the supercooled liquid layers, resulting in one model layer representing the mean properties of the liquid and ice cloud layers. It is therefore challenging to accurately represent thermodynamic properties and microphysical processes of mixed-phase clouds in climate models (Klein et al, 2009; Barrett, 2012).

Arctic temperature inversions and associated near-surface variables are poorly represented in current climate models. Medeiros et al (2011) analysed monthly-mean inversion strength across the models participating in the third phase of the Coupled Model Intercomparison Project (CMIP3), defining inversion strength as the difference between the 850 hPa and surface air temperature. Partitioning the data into land and ocean domains, they found a spread in typical inversion strengths on the order of 10 K, with many models overestimating stability over both land and sea ice. Their definition of inversion strength deviates from the textbook definition of an inversion as a layer of air where temperatures rise with altitude, but gives a robust estimate of the bulk stability of the lower troposphere consistent with the coarse vertical resolution of climate models. We therefore adopt the same definition for analyzing low-level stability as a proxy for inversion strength in model and reanalysis data throughout this paper. Turbulent fluxes at the surface are closely linked to the temperature structure and stability of the lower troposphere and also display a large spread in climate models. Medians of monthly mean turbulent heat fluxes over Arctic sea ice in winter range from -15 to +15 Wm^{-2} across different CMIP3 models, and the spread in net longwave radiative fluxes is of the same magnitude (Svensson and Karlsson, 2011).

The present study aims to understand the intermodel spread at the level of individual physical processes. Temperature inversions at high latitudes are a consequence of radiative cooling at the surface and advection of warmer air masses from lower latitudes (Zhang et al, 2011). To understand these processes, we use an idealised single-column experiment building on earlier studies by Wexler (1936) and Curry (1983). These studies show that radiative cooling, its interaction with cloud condensate and warm air advection are crucial not only for the development of temperature inversions but also that of the entire boundary layer and the surface heat budget in Arctic winter. Both Wexler (1936) and Curry (1983) refer to the radiative cooling of warmer air masses from maritime sources as formation of continental polar air. Throughout this paper, we will refer to the same process as formation of Arctic air masses.

Our investigation begins with an analysis of the large-scale monthly mean low-level stability in climate models and its relationship to global climate based on the results of Medeiros et al (2011) (Section 3). To understand what causes the spread and biases of low-level stability in models, we examine the processes governing the emergence of temperature inversions in Arctic winter. We show that the clear and cloudy states of the Arctic winter boundary layer correspond to different stages of the formation of Arctic air masses and analyse how low-level stability develops during this process (Section 4). Subsequently, observations of low-level stability for the clear and cloudy states of the boundary layer are compared to the sub-daily output of CMIP5 models (Section 5). Finally, we test the sensitivity of an idealised SCM experiment of Arctic air formation to different model parametrisations in order to relate biases in global models to individual processes (Sections 5.1 and 5.2).

2 Models and data

Monthly mean atmospheric and near-surface air temperatures as well as sensible heat fluxes from the historical runs of a range of CMIP5 models (Table 1) and from the RCP8.5 runs for a subset of models based on data availability are used for the analysis of large-scale low-level stability and fluxes (Taylor et al, 2012). A more detailed analysis is carried out for the models for which we could obtain both atmospheric and near-surface temperatures and surface net longwave radiation at sub-daily resolutions. These models are listed alongside a brief characterisation of their mixed-phase cloud microphysics parameterisations in Table 2.

Observations made in multiyear pack-ice north of Alaska between October 1997 and October 1998 have been obtained from the SHEBA experiment (Persson et al, 2002). Standard meteorological observations and flux measurements were made on the ice floe, while atmospheric profiles were obtained from six- to twelve-hourly launches of radiosondes. We further use surface observations and radiosonde profiles from the Atmospheric Radiation Measurement (ARM) site in Barrow at the north coast of Alaska at 71.3°N 156.6°W (Xie et al, 2010).

We use reanalysis data from both the ERA-40 (Uppala et al, 2005) and the updated ERA-Interim dataset (Simmons et al, 2007). The two reanalyses use different versions of the European Center for Medium-Range Weather Forecasts' integrated forecast system and different data assimilation schemes. Since all reanalyses rely on the assimilation of observations, results are less reliable for regions with scarce observational data such as the Arctic (e.g. Sorteberg et al, 2007). Given the lack of regular surface observations and soundings over the Arctic ocean, the reanalyses' vertical temperature profiles will strongly depend on satellite retrievals and the model used to derive the reanalysis. Tjernström and Graversen (2009) found a near-surface warm bias of about 1K in ERA-40 compared to SHEBA data that persisted despite the assimilation of SHEBA observations into the reanalysis. Comparing ERA-40 first-guess values and final analyses for the SHEBA years and years without assimilated soundings, they concluded that assimilating the soundings reduced the near-surface warm bias by about 0.5 K. While this limitation should be considered when using reanalyses to evaluate climate models, Tjernström and Graversen (2009) suggest that ERA-40 somewhat underestimates typical inversion strengths, but properly captures the climatological characteristics of temperature inversions. We will show later that climate model biases are much greater than the likely error of the reanalysis, which justifies using the latter as approximation of the observational "truth".

2.1 Single-column models, forcing and initialization

We use a single-column framework to model the cooling of an air mass advected from lower latitudes into the Arctic in winter (Wexler, 1936; Curry, 1983). By applying a Lagrangian perspective, i.e. following the trajectory of the air mass with the single-column model and assuming horizontal homogeneity, we devise an idealised setup to study the role of local processes. Large-scale advection of heat and moisture plays an important role in the formation and resilience of mixed-phase clouds and is the basis of our Lagrangian setup. We neglect the role of open leads which are sources of heat and moisture (Andreas et al, 2002).

Most experiments are run with the single-column version of ECHAM6, the atmosphere component of MPI-ESM (Stevens et al, 2013). We choose a vertical resolution of 47 layers as used in the CMIP5 runs with MPI-ESM-LR to be able to compare our SCM results to climate model output. The lowest level is located approximately 30 m above the ground and there are 10 levels within the lowest 3 km. Some

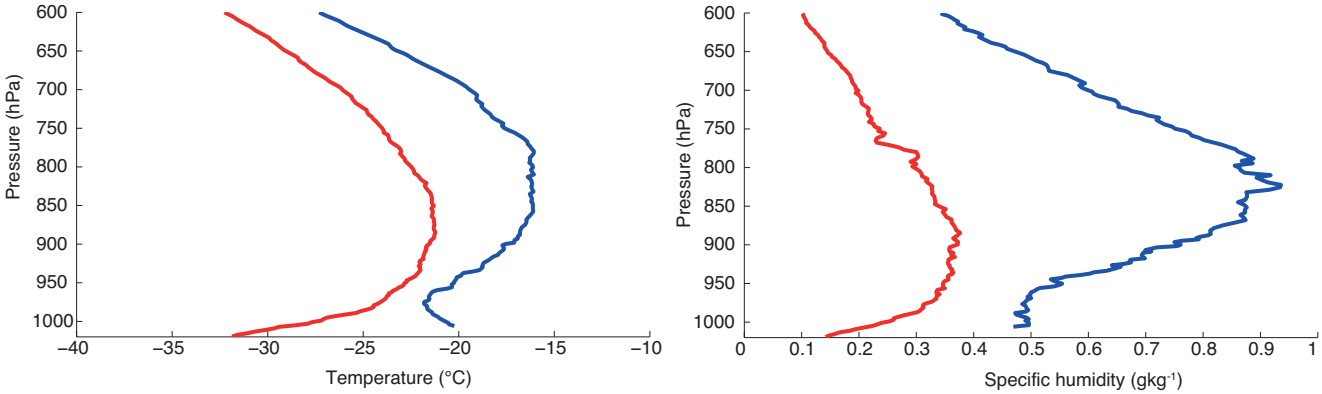

Fig. 2 Median vertical structures of temperature and humidity in the clear (red) and cloudy (blue) boundary layer observed NDJF during SHEBA. Redrawn following Stramler et al (2011) using a threshold of -10 Wm^{-2} of surface net longwave radiation to separate the two states.

Table 1 CMIP5 models used in this study

Model	Modelling centre
BCC-CSM1-1	Beijing Climate Center
BNU-ESM	College of Global Change and Earth System Science, Beijing Normal University
CanCM4	Canadian Centre for Climate Modelling and Analysis
CMCC-CM	Centro Euro-Mediterraneo per I Cambiamenti Climatici
CNRM-CM5	Centre National de Recherches Météorologiques
CSIRO-Mk3-6-0	Commonwealth Scientific and Industrial Research Organization
EC-EARTH	EC-EARTH consortium
FIO-ESM	The First Institute of Oceanography
FGOALS-s2	LASG, Institute of Atmospheric Physics
GFDL-CM3	NOAA Geophysical Fluid Dynamics Laboratory
GISS-E2-R	NASA Goddard Institute for Space Science
INMCM4	Institute for Numerical Mathematics
IPSL-CM5A-LR	Institut Pierre-Simon Laplace
IPSL-CM5B-LR	Institut Pierre-Simon Laplace
MIROC-ESM	Japan Agency for Marine-Earth Science and Technology
HadCM3	Met Office Hadley Centre
MPI-ESM-LR	Max Planck Institute for Meteorology
MRI-CGCM3	Meteorological Research Institute
CCSM4	National Center for Atmospheric Research
CESM1-CAM5	Community Earth System Model Contributors
NorESM1-M	Norwegian Climate Centre

experiments are repeated with the single-column version of the Community Atmosphere Model version 4 (CAM4, Gent et al, 2011), which is the atmosphere component of CCSM4.

The cloud microphysics scheme of ECHAM6 treats cloud water and cloud ice as separate prognostic variables, while rain and snow are diagnosed. Instantaneous homogenous freezing of all cloud liquid water is assumed at temperatures below -35 °C, while stochastic heterogenous and contact freezing occur at temperatures between 0 and -35 °C. Cloud ice may be transferred to lower levels or the surface through sedimentation, converted into snow by aggregation and accretion, and sublimated or melted. Details of the scheme are described in Lohmann and Roeckner (1996).

The initial temperature profile represents an air mass in equilibrium with a near-freezing ocean surface. Temperature is prescribed as $T = T_0 \left(\frac{p}{p_0} \right)^{R\gamma g^{-1}}$ below 300 hPa and constant above that level, where $T_0 = 273$ K and $p_0 = 1013$ hPa are the surface temperature and pressure, $\gamma = 8 * 10^{-3}$ Km^{-1} is the assumed lapse rate, $R = 287$ $Jkg^{-1}K^{-1}$ the gas constant for air and g gravitational acceleration (Curry, 1983). Relative humidity drops linearly with pressure from 80 percent at the surface to 20 percent at 600 hPa. A constant specific humidity of $3 * 10^{-6}$ is prescribed between 300 hPa and the model top. The model location is set to 70 °N, initial sea ice thickness is 1 m and initial snow cover 0.1 m water

equivalent. A geostrophic wind of 5 ms^{-1} is prescribed up to 300 hPa in order to drive moderate turbulent mixing. Large-scale advection of heat, moisture and momentum are set to zero. CO_2 concentration is set to the preindustrial value of 280 ppm. Surface temperatures are initialized at 250 K, the ocean underneath the ice is assumed to be at the freezing point of sea water (-1.9°C). Surface temperatures, sea ice and snow properties are calculated interactively during the experiment. The model is started on 1 January and run for 20 days, leading to zero insolation throughout the experiment.

The qualitative results described in this study are robust to small changes in the initial and boundary conditions such as the initial surface temperature, initial temperature profiles and the prescribed geostrophic wind profile. Since the formation of clouds depends on the initial relative humidity profile, we prescribe a relative humidity quickly dropping off with increasing altitude to study low-level cloud processes over several days while avoiding high-level cloud formation.

Table 2 Overview of CMIP5 models providing high-frequency data. a)T_t: triple point, ΔT=11.82 K b) T_0=-4°C over ocean and -10°C over land.

CMIP model	Atmosphere	No. of layers	Reference	Computation of cloud ice fraction f
BCC-CM-1-1	BCC-AGCM 2.0.1	26	Wu et al (2010)	Linear between -10 and -40
CMCC-CM	ECHAM5	31	Scoccimarro et al (2011)	Explicit parameterisation of freezing processes between 0 and -35
CCSM4	CAM4	26	Gent et al (2011)	Linear between -10 and -40
CNRM-CM5	Arpege-Climat 5.1	31	Météo France (2009)	No prognostic condensate, $f = 1 - exp\left\{\frac{-1}{2(\Delta T)^2}(T - T_t)^2\right\}$ [a]
GISS-E2-R	GISS ModelE	40	Schmidt et al (2006)	T-dependent probability of freezing and Bergeron-Findeisen process $p_i = 1 - exp\left[-\left(\frac{T_0 - T}{12}\right)^2\right]$ [b]
GFDL-CM3	GFDL-AM3	48	Donner et al (2011)	Explicit parameterisation of freezing processes between 0 and -30, almost no water at temperatures colder than -15
INMCM4	INMCM	21	Volodin et al (2010)	$f = 1 - (0.0059 + 0.9941 \cdot exp(-0.003102T^2)$
IPSL-CM5A	LMDZ5A	39	Hourdin et al (2012)	Linear between 0 and -15
MIROC-ESM	MIROC-AGCM	80	Watanabe et al (2011)	$f = 1 - exp((-((268.91K - T)/12K)^2))$ above $-38°C$
MPI-ESM-LR	ECHAM6	47	Stevens et al (2013)	Explicit parameterisation of freezing processes between 0 and -35
MRI-CGCM3	MRI-AGCM3	40	Yukimoto et al (2012)	Explicit parameterisation of freezing processes, Bergeron-Findeisen process triggers full and immediate glaciation if ice water content > 0.5 mg kg^{-1}

3 Lower tropospheric temperature structure in CMIP5 models

We assess the typical temperature structure of the Arctic wintertime boundary layer and lower troposphere by analysing the area-weighted pdfs of monthly mean low-level stability over land and ocean from CMIP5 models and reanalyses (Figure 3). We obtain a similar bimodal distribution over the ocean domain as Medeiros et al (2011) did for CMIP3 with a stable mode over sea ice and a near-neutral mode over open water. The distribution between the two modes essentially reflects the different sea-ice cover between models, and models do agree on the temperature structure of the near-neutral mode (-12 to -8 K) within a few Kelvin. Over the ocean, we will therefore focus on the stable mode that corresponds to the sea-ice covered Arctic ocean and contains the bulk of the inter-model spread.

Mean modelled low-level stability in the stable mode range from about 1.5 K to 13 K (Figure 4), while reanalyses give 4.1 (ERA-int) and 4.9 K (ERA40). Only five models produce weaker stability than the reanalyses, while 15 models produce stronger stability. The distribution of low-level stability over land is unimodal with a somewhat smaller intermodel spread (Figure 3b), mean modelled stability between 4.5 K and 11.5 K and reanalyses values of 7.1 (ERA40) and 7.5 K (ERA-int). Eight models display smaller and ten models larger stability than the reanalyses. In the reanalyses, mean low-level stability over land are 2 to 3 K stronger than over the ocean, while the difference is less than one K for most models. Five models display a difference of at least 2 K, and five other models display stronger stability over the ocean than over land.

Models with strong stability are underrepresented in the high-frequency output sample (Table 2), as can be seen in the distribution of dashed and solid lines in Figure 3. Reanalyses data should be used with caution because observational data over the Arctic ocean are limited to satellite irradiances and sporadic observational campaigns. If we assume the surface warm bias of up to 1.5 K detected in ERA40 compared to SHEBA observations (Tjernström and Graversen, 2009) to be representative of the entire Arctic ocean and the whole time period considered, five models would fall within the range of realistic values, while ten models would still overestimate mean low-level stability. Since more soundings are available over land than over the Arctic ocean, the reanalysis bias over land could be smaller, leading to an overestimate over land-sea contrasts in low-level stability by the reanalysis.

Within an individual climate model, mean Arctic low-level stability is closely related to global mean temperature (Figure 5). Given the previously described amplification of Arctic warming near the surface, this relationship can be explained in simple terms. In a warming climate, the Arctic surface warms faster than air aloft, which leads to a weakening of temperature inversions and reduced low-level stability. This reduction of atmospheric stability and disappearance of temperature inversions is a prerequisite for deep convection over the Arctic ocean in winter, which has been suggested as a mechanism keeping the Arctic ocean free of winter sea ice in warm climates (Abbot and Tziperman, 2008).

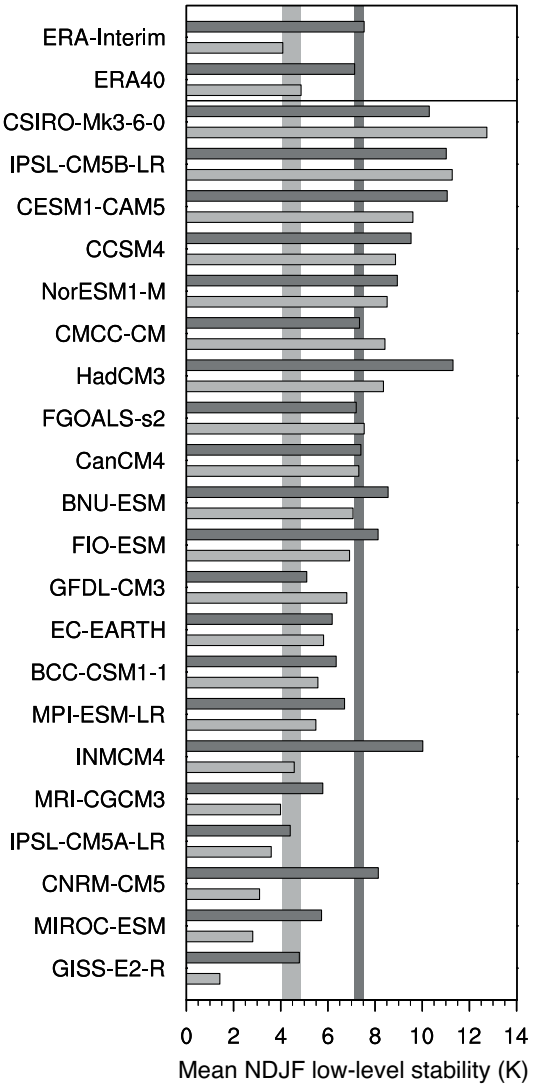

Fig. 4 Mean low-level stability in the stable mode over the ocean (light gray) and over land (dark gray). Models are sorted by mean low-level stability in the stable mode over ocean. Modes are separated at the local minimum of the pdf for each model. Shaded areas mark the range of the reanalyses.

Since global mean temperatures are cold-biased in most climate models (Mauritsen et al, 2012), their relationship to Arctic low-level stability could in principle explain some of the overestimation relative to reanalyses of present-day stability noted before. However, Figure 5 shows that while the models with the strongest stability also tend to be cold-biased, this relationship cannot explain the bulk of the inter-

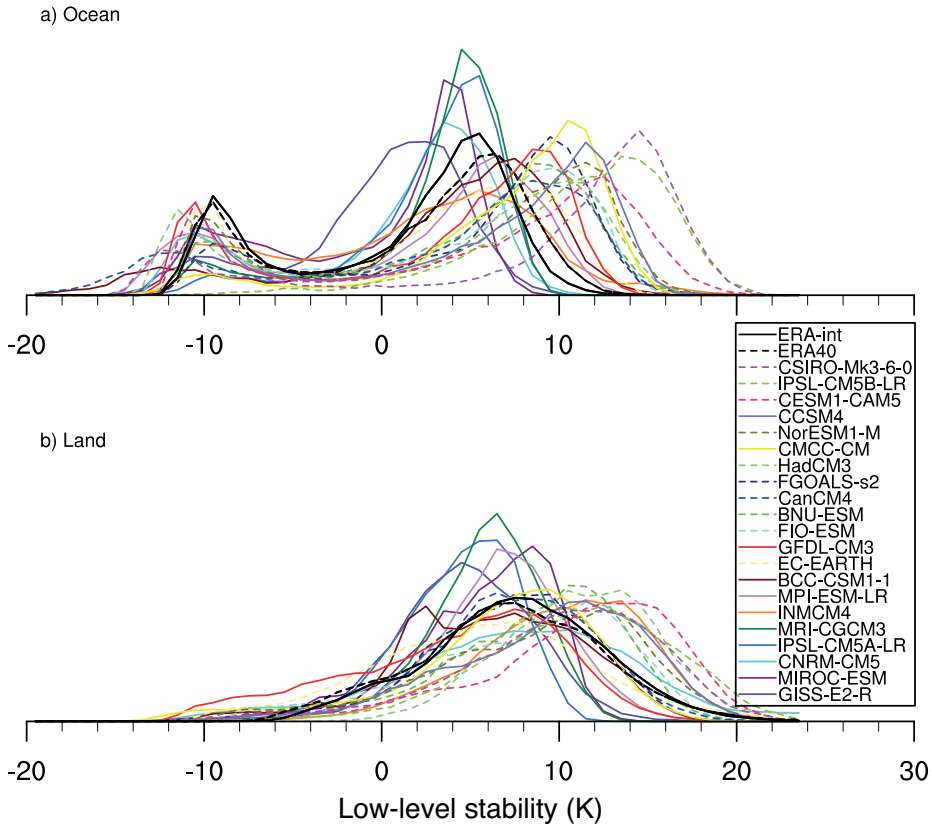

Fig. 3 PDFs of NDJF Arctic (north of 64 °N) monthly mean grid-point wise low-level stability in the historical runs, 1990-1999. Inversion strength is defined as 850 hPa temperature minus surface air temperature. The models' own land-sea masks have been used to partition data into land and ocean domains, considering any gridpoint with more than 20 percent land fraction as land. Models from Table 2 are displayed with solid lines.

model spread. To understand the spread of results, we thus need to investigate the local processes that control the emergence and strength of temperature inversions in Arctic winter.

4 The formation of Arctic air masses

Building on Wexler (1936) and Curry (1983), we investigate the formation of Arctic air by following a relatively warm and moist air mass from lower latitudes that is advected over cold Arctic sea ice. We model the air mass transformation in a SCM experiment as described in section 2.1.

Initially, an inversion is formed (Figure 7a) and the air mass cools to space and to the surface (Figure 6a). Radiative cooling leads to saturation of the air and the formation of liquid or mixed-phase clouds. Because the emissivity of these clouds is close to unity, radiative cooling now occurs in the cloud layer rather than at the surface, progressively eroding the inversion and reducing low-level stability (b). The cloud cools and is eventually transformed from a mixed-phase to a low-emissivity ice cloud, which allows the surface to cool radiatively (c). When the condensate has fallen out, strong surface cooling under a clear sky leads to the emergence and growth of a new surface-based temperature inversion (d). In the SCM experiment, (a) and (c) are unstable states in rapid transition to the quasi-stable state (b) or the stable state (d). Observations of both supercooled liquid water and ice clouds in the same temperature range indicate that the transition from a mixed-phase cloud (b) to an ice cloud (c) does not represent a threshold behaviour that occurs at a given temperature, but rather a regime shift in the dynamical interactions between cloud microphysics, cloud macrophysics and environmental conditions (Morrison et al, 2012). The formation of Arctic air leads to the formation of a humidity inversion (Figure 8) that is characteristic for the cloudy state of the boundary layer (Figure 2) because condensation begins near the surface and occurs at increasing altitudes as the boundary layer cools.

The first quasi-stable state (b) with little to no surface cooling in the presence of mixed-phase clouds corresponds to the cloudy state found in SHEBA observations, while the second stable state (d) with strong longwave cooling in the absence of cloud liquid water corresponds to the clear state (Persson et al, 1999, 2002; Stramler et al, 2011). The occurrence of both states of the Arctic wintertime boundary layer is reflected in the bimodal distribution of surface net

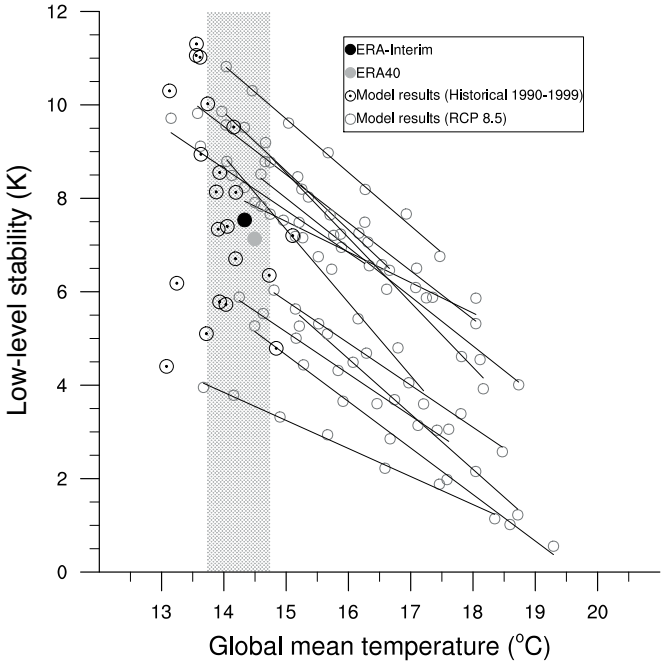

Fig. 5 Mean low-level stability over land against global mean temperature in models and reanalyses. Lines show regressions within the RCP8.5 runs of a subset of models, black circles represent all CMIP5 model shown in Figure 4. The dotted area shows observed global mean temperatures and the associated uncertainty according to Jones et al (1999).

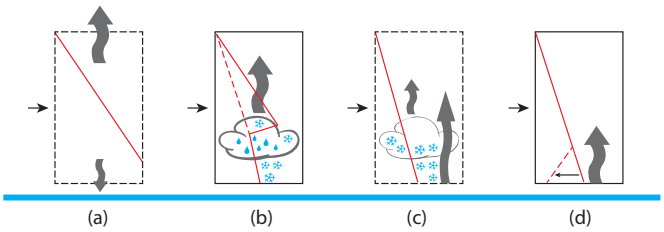

Fig. 6 Sketch of the formation of Arctic air. Dashed boxes mark unstable transition states.

longwave radiation during the SCM experiment described in section 2.1 (Figure 9). Despite the highly idealized nature of the experiment, the location of the peaks matches those obtained from SHEBA observations. This indicates that the net surface longwave radiation in the two states of the Arctic winter boundary layer is an emergent property of the coupled surface-atmosphere system that is captured by the SCM, and largely independent of the actual temperatures and large-scale forcings. Note that since the SCM remains in the clear state at the end of the experiment, the relative weight of each peak depends on the duration of the model run and should not be compared to observations. The single-column experiment also reproduces the observed link between the presence of cloud liquid water and the ocurrence of the cloudy state (Figure 9, Tjernström, 2012). The mechanism described here is consistent with observations of Arctic air mass formation in nortwestern Canada (Turner

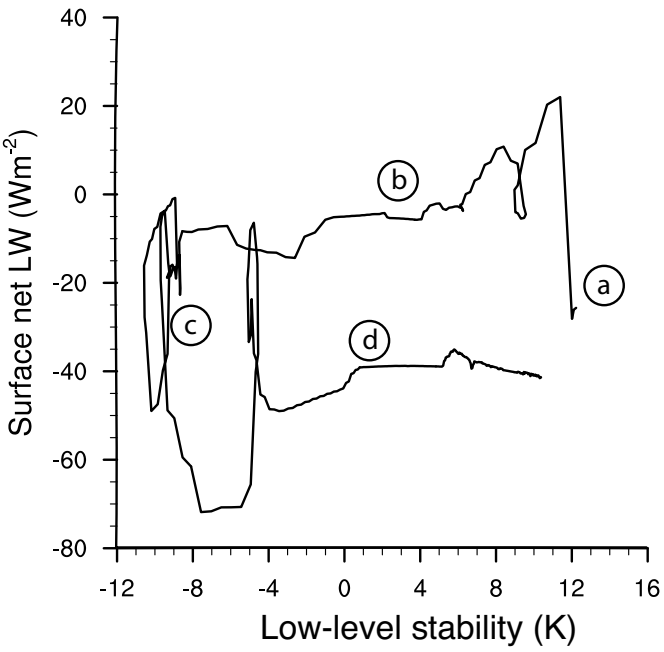

Fig. 7 Trajectory of low-level stability against surface net longwave radiation in idealized SCM experiment of Arctic air formation (section 2.1), hourly averages.

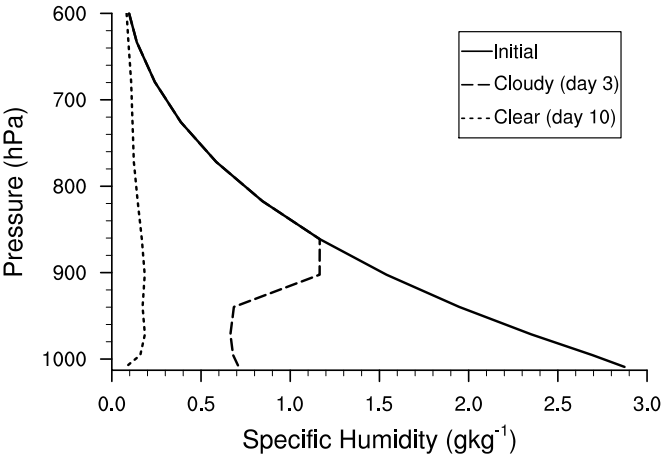

Fig. 8 Profiles of specific humidity during the SCM experiment.

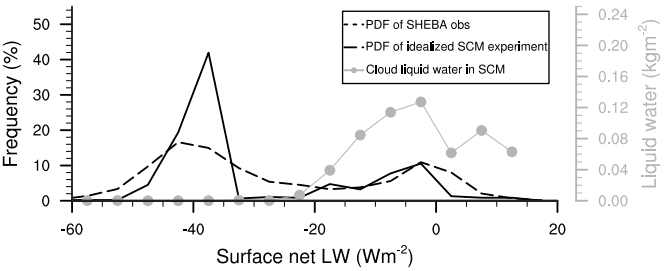

Fig. 9 PDF of surface net longwave radiation during the formation of Arctic air in ECHAM6 SCM and observed NDJF at the SHEBA site. Both time series are hourly averages, bins are 5 Wm^{-2} wide. Grey circles denote cloud liquid water paths averaged for each bin.

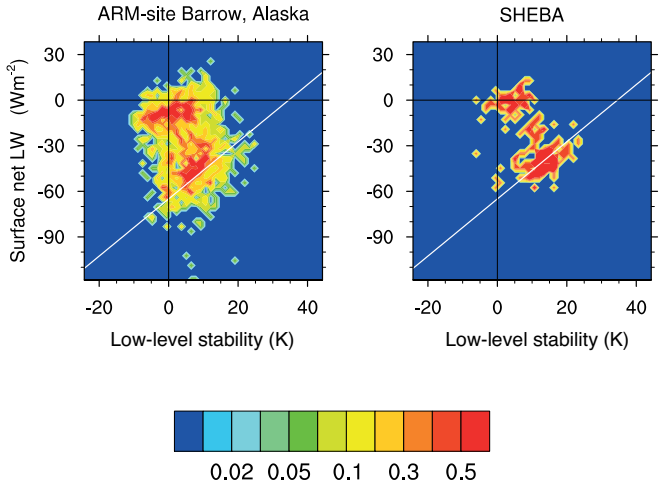

Fig. 10 Bivariate pdfs of NDJF low-level stability and surface net longwave radiation from SHEBA observations (1997/1998) and the ARM site in Barrow (2000-2009). Low-level stability is defined as the temperature difference between the 850 hPa level and the near-surface air. Temperature measurements are for individual soundings while surface radiation measurements are 6-hourly averages. The pdf is constructed using 50 by 50 equally spaced bins ranging from -25 to 45 K for low-level stability and from -120 to 40 W m^{-2} for net longwave radiation. The white line drawn across the plot serves as a visual reference and indicates a relationship between surface cooling and low-level stability with a Stefan-Boltzmann equation linearised around 240 K and assuming an effective atmospheric emissivity of 0.6. Both values are chosen to visually match the position and slope of the maximum density region in the pdfs.

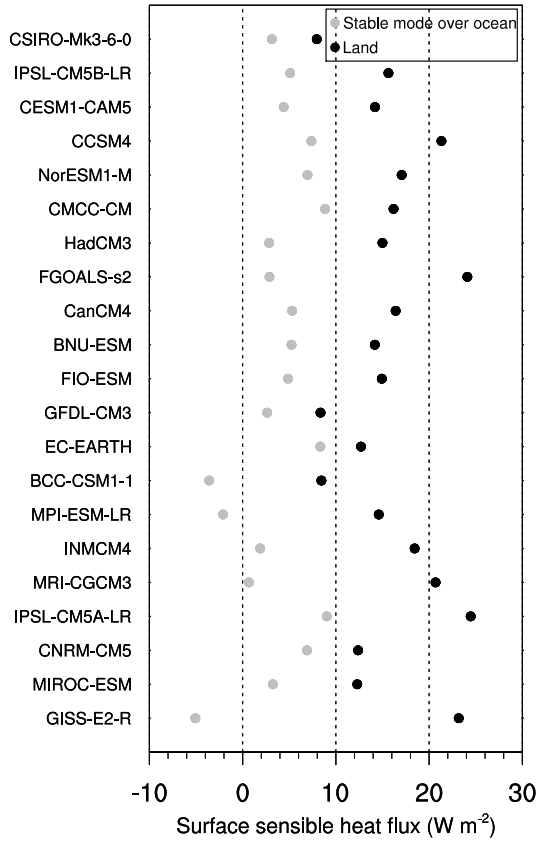

Fig. 14 Arctic NDJF monthly mean turbulent heat fluxes in CMIP5 models 1990-1999, positive downwards.

and Gyakum, 2011), where cloud-top radiative cooling preceded clear-sky surface radiative cooling and the formation of surface-based temperature inversions.

Having established how temperature inversions develop and decay during the clear and cloudy states of the Arctic winter boundary layer, we proceed to analyse how the representation of these states affects mean low-level stability in global climate models.

5 The two states of the boundary layer in observations and CMIP5 models

Arctic wintertime inversions in the clear state of the boundary layer are typically stronger than in the cloudy state, as can be seen in ARM and SHEBA observations (Figure 10). Within the clear state, stronger stability correspond to weaker longwave cooling. These observations are consistent with the processes outlined in the previous section and illustrated in Figure 6.

To determine to what extent the overestimation of mean low-level stability in models compared to reanalyses is caused by shortcomings in the representation of one or both states and by the distribution between the states, we analyse the distribution of low-level stability and surface radiative cooling in sub-daily output of CMIP5 models. While we cannot expect Arctic-wide model output to match point observations, models should represent the qualitative behaviour of a bimodal distribution with different stability between modes. Station output at high frequency would in principle allow for a closer comparison of model and observational data, but was only available for a few models.

The models can be grouped into three categories (Figures 11 and 12):

1. Three models (BCC-CSM-1-1, CMCC-CM and MPI-ESM-LR) reproduce the bimodal behaviour of the Arctic winter boundary layer with distinct clear and cloudy states as well as stronger stability in the clear than the cloudy state. CMCC-CM has a less frequent cloudy state and stronger mean stability than BCC-CSM-1-1 and MPI-ESM-LR, which both have stability about 1 K stronger than the reanalyses over the ocean and weaker than the reanalyses over land (Figure 4).

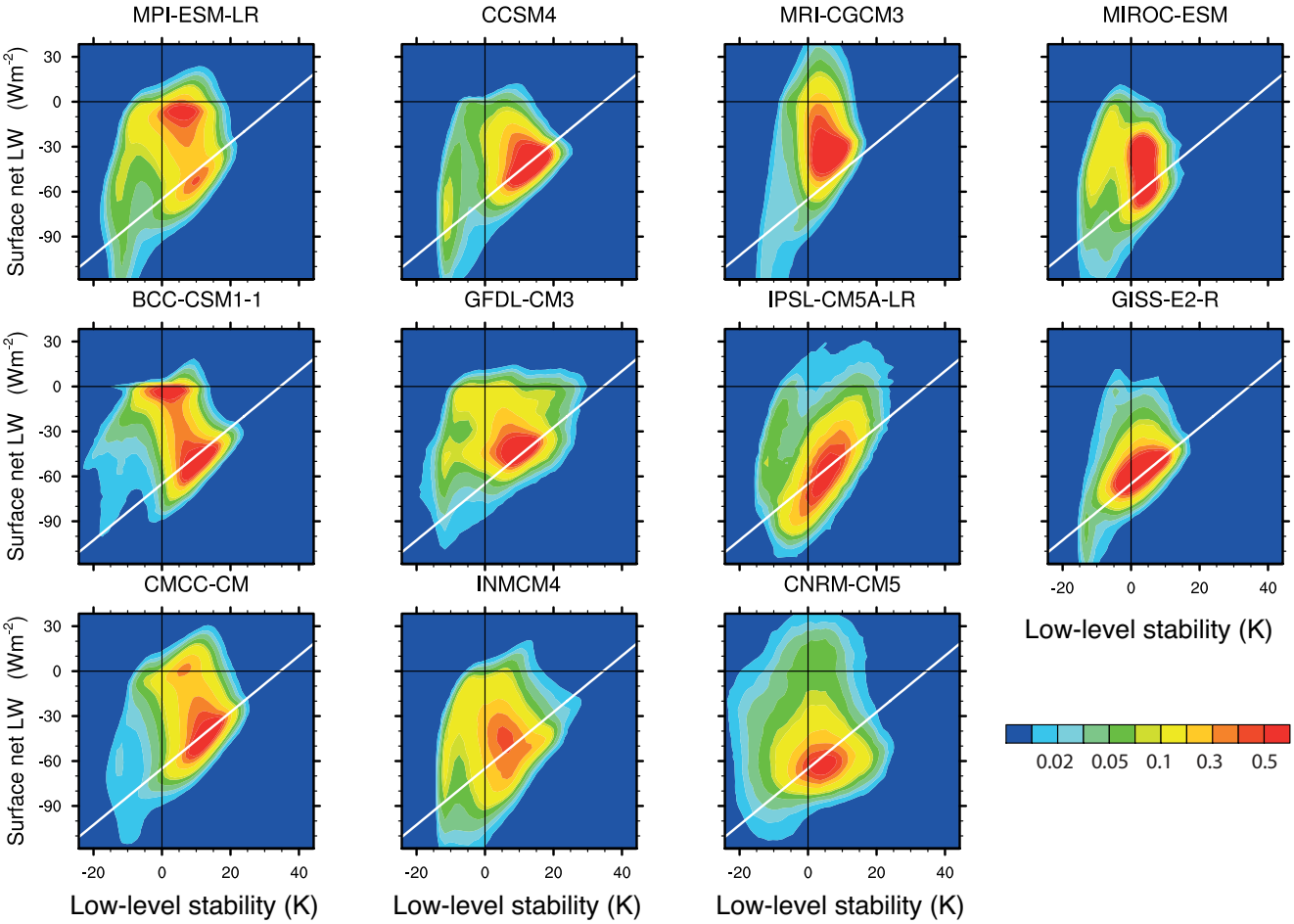

Fig. 11 Bivariate pdfs of NDJF low-level stability and surface net longwave radiation from CMIP5 models, 6-hourly values from the ocean area north of 64 °N for 1990-1999 of the historical runs.

2. Three models (CCSM4, GFDL-CM3 and INMCM4) lack the cloudy state, out of which CCSM4 over both ocean and land, GFDL-CM3 over ocean and INMCM4 over land produce stronger mean stability than the reanalyses. GFDL-CM3 is one of very few models with stronger stability over the ocean than over land, while INMCM4 mean low-level stability are in agreement with the reanalyses over ocean and much stronger than the reanalyses over land.
3. Five models lacking the cloudy state produce weak stability despite strong longwave cooling. These models also produce weaker monthly mean stability than the reanalyses. We will show later that this can be caused by excessive downward sensible heat fluxes from the atmosphere or excessive upward conductive heat fluxes from the liquid ocean to the surface.

Some models that do not represent the cloudy state over the ocean do so over land. This is most evident in INMCM4, but also in GFDL-CM3, CNRM-CM5 and IPSL-CM5A which all show a distinct but small representation of the cloudy state over land.

We can explain some of the relationships between boundary layer state, low-level stability and surface heat fluxes (Figure 13 and 14) in different CMIP5 models. MPI-ESM-LR and BCC-CSM1-1 typically produce small upward monthly mean sensible heat fluxes over sea ice, while most other models including CMCC-CM produce mean downward turbulent fluxes (Figure 13). SHEBA observations show that upward turbulent fluxes indeed occur in the cloudy state, when the surface does not cool radiatively but is still warmed through conductive heat fluxes from the warmer ocean surface underneath the ice (Persson et al, 2002). We can therefore understand that models lacking the cloudy state predominantly produce downward sensible heat fluxes in a stably stratified boundary layer that is associated with surface radiative cooling.

IPSL-CM5A has the strongest downward sensible heat fluxes over both land and ocean, which explains the models' very weak stability despite strong longwave cooling. Interestingly, the introduction of a new physics package in IPSL-CM5B has substantially changed the inversion characteristics, reducing downward turbulent heat fluxes and making

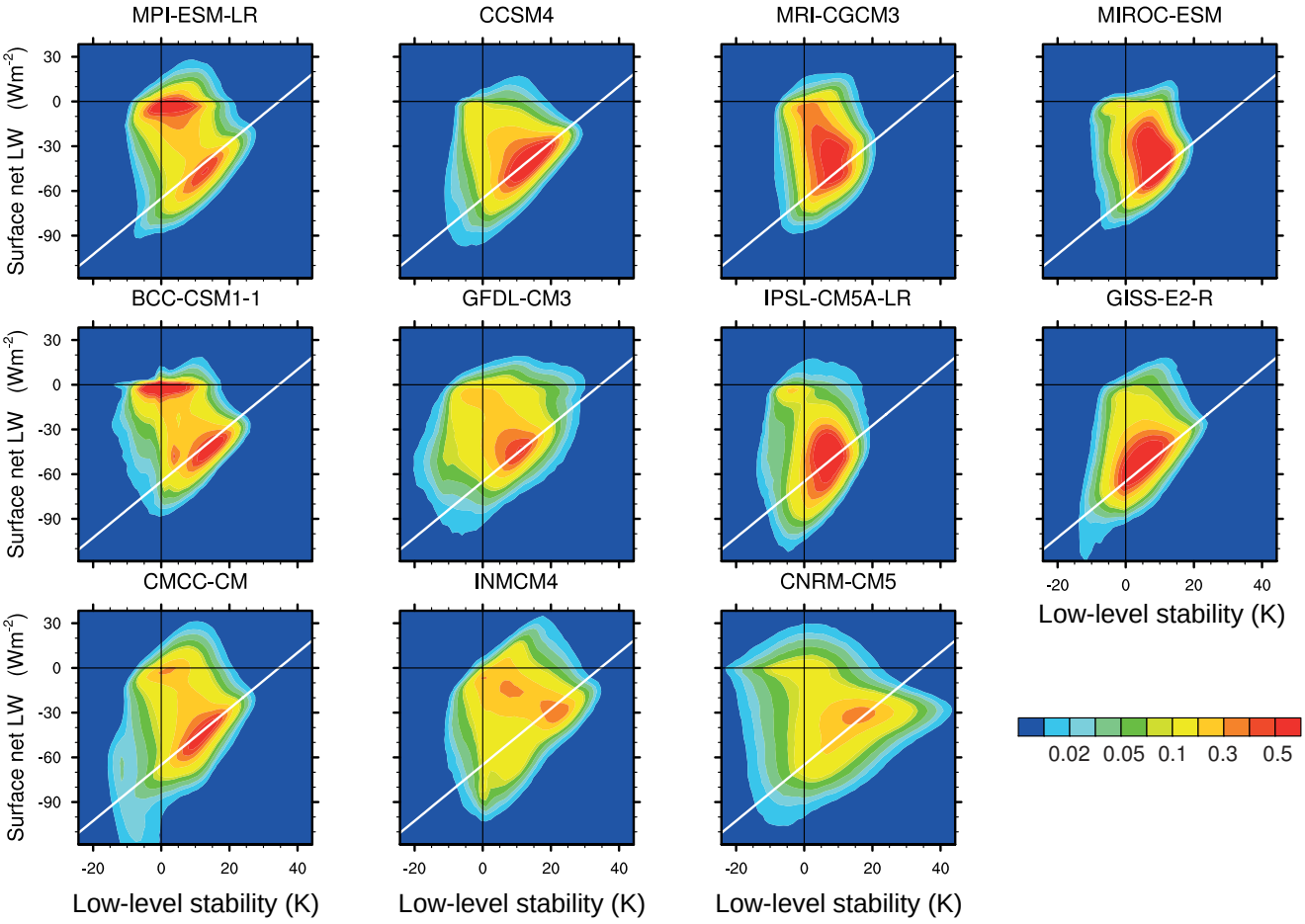

Fig. 12 Bivariate pdfs of NDJF low-level stability and surface net longwave radiation from CMIP5 models, 6-hourly values over land.

the model produce one of the strongest mean stability in the ensemble (Figure 4). Unfortunately, no sub-daily data from IPSL-CM5B were available for this study.

As noted before, most models have smaller land-ocean contrasts in low-level stability than reanalyses and much stronger downward sensible heat fluxes over land than over the ocean. In contrast to sea ice, the land surface is not warmed from below, which could explain stronger stability over land than sea ice. The much stronger sensible heat fluxes towards the land surface in models might be related to models overestimating diffusivity under strongly stable stratification (Cuxart et al, 2006), weakening the land-ocean contrast in low-level stability. Land-ocean contrasts in low-level stability are larger than in reanalyses in CNRM-CM5 (Figure 4), likely due to sensible heat fluxes being virtually identical over both surfaces.

The GISS-E2-R model stands out by having monthly mean turbulent fluxes similar to models that do represent the cloudy state (Figure 13), but by far the weakest stability over sea ice (Figure 4) while producing strong surface longwave cooling at all times (Figure 11). Over land, the GISS-E2-R model displays strong downward turbulent fluxes and stability at the lower end, but within the range of other models. We infer that the upward turbulent fluxes and very weak stability over the ocean are caused by strong conductive heat fluxes from the ocean that effectively prevent the boundary layer from becoming very stably stratified.

Eight of eleven analysed models lack a distinct representation of the cloudy state of the Arctic winter boundary layer over sea ice and therefore produce excessive surface longwave cooling. The few models that do represent a distinct cloudy state also have monthly mean low-level stability in better agreement with reanalyses. Models with excessive longwave cooling caused by the lack of a cloudy state may either produce strong stability or compensate for the cooling by stronger turbulent or conductive heat fluxes towards the surface, which results in weak low-level stability. It should be noted that models lacking the cloudy state do not display a cloud-free Arctic ocean, but merely lack near-surface liquid or mixed-phase clouds that have a large enough emissivity to inhibit surface longwave cooling. In other words, the issue with models is not their cloud fraction but their cloud phase. We thus find that the bias of too little liquid

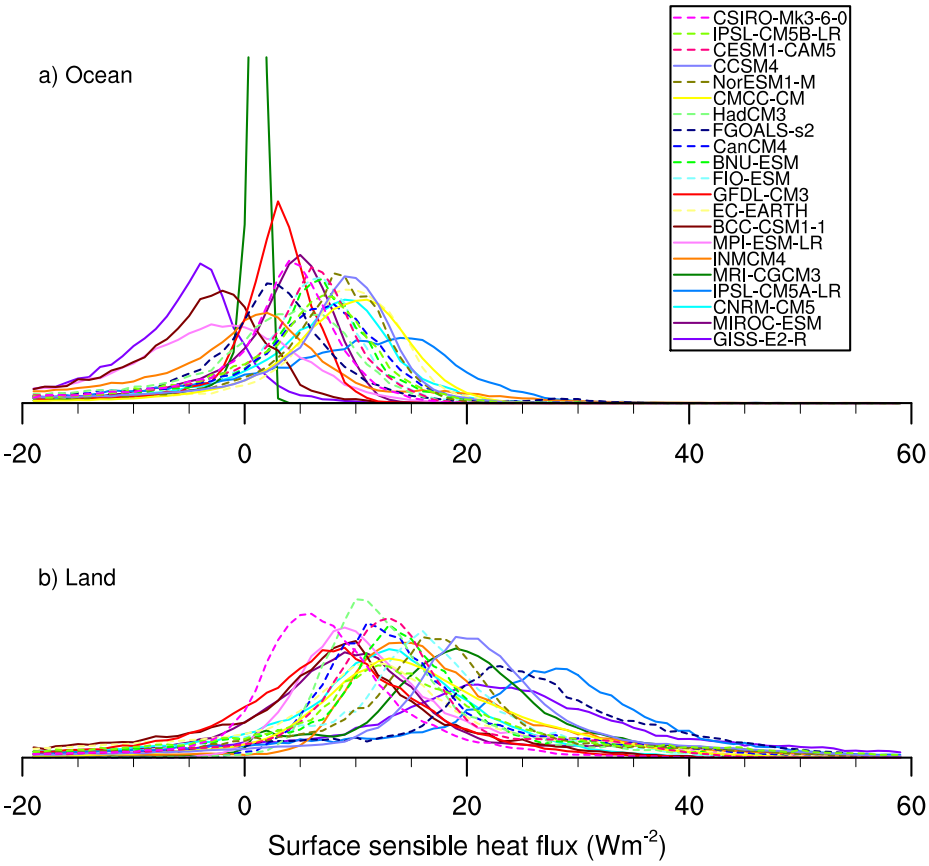

Fig. 13 PDF of Arctic NDJF monthly mean turbulent heat fluxes in CMIP5 models 1990-1999, positive downwards. Downward turbulent fluxes over sea ice in the MRI-CGCM3 model are always very small over sea ice, which results in the narrow peak at small positive values in Figure a.

water in Arctic winter clouds found by Cesana et al (2012) for IPSL-CM5B does occur in a wide range of models.

5.1 The role of mixed-phase cloud microphysics

To link this process-based understanding of the climate models' mean state to individual model parameterisations, we perform sensitivity experiments using the SCM. Since the presence of cloud liquid water is important for determining the surface longwave radiation balance and thus the state of the Arctic boundary layer, the representation of mixed-phase cloud microphysics at low temperatures is likely to be an important process. Many CMIP5 models prescribe a temperature-dependent ratio of ice to total condensate (Figure 15). The atmosphere component of MPI-ESM-LR, ECHAM6, instead computes temperature-dependent freezing rates. For this model, ratios of ice to total condensate during the SCM experiment are plotted for comparison.

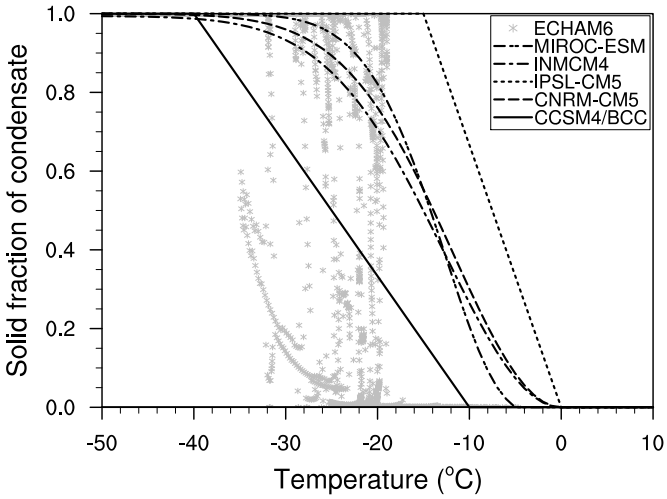

Fig. 15 Temperature dependence of condensate phase in different CMIP5 models.

To test model sensitivity to changes in cloud microphysics, we modify the respective parameterisation in MPI-ESM-LR to mimic the behaviour of the other schemes shown in Figure 15 and re-run the single-column experiment. For all schemes except the one used in CCSM4 and BCC-CSM-1-1, which allows for a substantial fraction of cloud liquid water at cold temperatures, this leads to the disappearance of the cloudy state (Figure 16), showing that freezing of cloud liquid water at too warm temperatures can explain the lack of a cloudy state in the analyzed models except for CCSM4. The phase

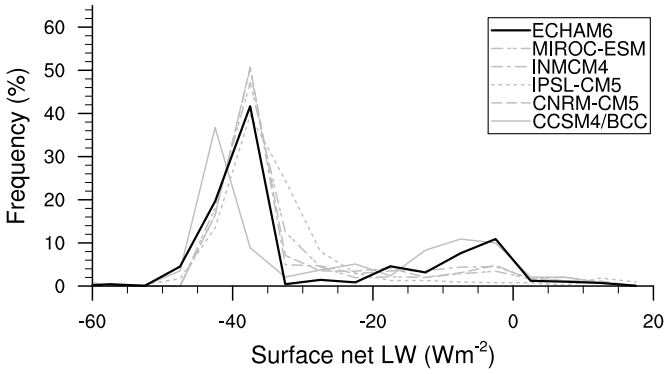

Fig. 16 PDFs of surface net longwave radiation in SCM experiment with perturbed microphysics.

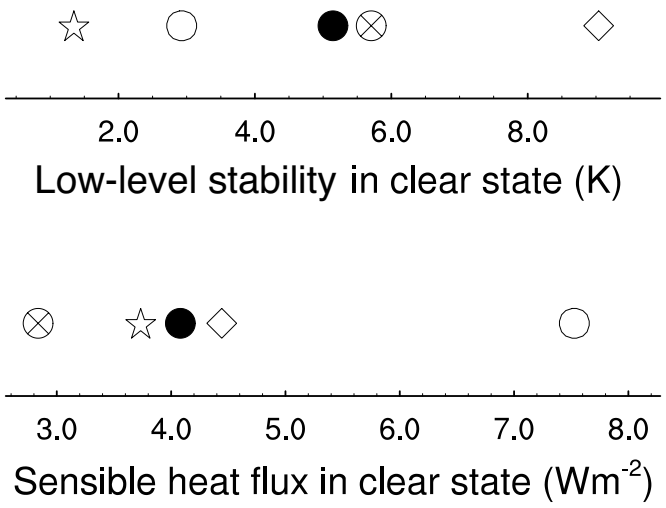

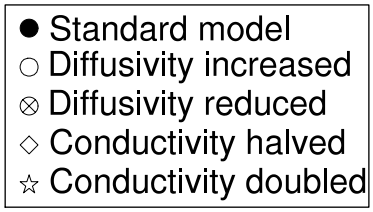

Fig. 17 Overview of parameterisation sensitivity experiments in SCM. The clear state is defined as all timesteps with surface net longwave radiation below -20 Wm^{-2}

of condensate is computed in the same way in CCSM4 and BCC-CSM-1-1, but the latter model does represent the cloudy state in agreement with our SCM experiment. The lack of the cloudy state in CCSM4 could be caused by other parameterisations, implementation issues or different large-scale conditions. In runs done with the single-column version of CCSM4, vertically integrated total cloudiness never exceeds 0.4, while it is unity during almost the entire experiment in ECHAM6 (not shown). This difference in the modelled cloud cover contributes to continuous surface radiative cooling on the order of 40 Wm^{-2} in CCSM4, supporting the suggestion that mechanisms other than the mixed-phase cloud microphysics parameterisation are responsible for the lack of a cloudy state in this model. We could not test the more complicated parameterisations of the GFDL-CM3, GISS-E2-R and MRI-CGCM3 models in the same way, but it is known that the freezing parameterisation in the GFDL-CM3 model leads to an almost complete disappearance of cloud liquid water below -15 °C (Rotstayn et al, 2000). The MRI-CGCM3 model has a parameterisation of the Bergeron-Findeisen process that leads to immediate freezing of all condensate as soon as cloud ice exceeds a threshold value of 0.5 mg kg^{-1} (Yukimoto et al, 2012), which is exceeded immediately once freezing begins in ECHAM6. It is therefore likely that these parameterisations also result in a rapid transition to ice clouds. In the GISS-E2-R model, there is a temperature-dependent probability for freezing to occur at any timestep plus a representation of the Bergeron-Findeisen process, which likewise make rapid glaciation very likely to occur (Schmidt et al, 2006).

Modifying one parameterisation of a single model to resemble the behaviour of other models is of course no substitute for a full model intercomparison, as we also see in the differing results between CCSM4 itself and the version of ECHAM6 modified to resemble CCSM4 mixed-phase cloud microphysics. However, our experiments show that the differences in cloud microphysics among CMIP5 models can determine the presence or lack of a cloudy state during Arctic air formation, all other things being equal.

5.2 Model sensitivity to turbulent diffusivity and heat conduction

Amongst models lacking a realistic representation of mixed-phase clouds, typical monthly-mean low-level stability still varies between 1.5 and 10 K (Figure 4). Under radiatively clear sky conditions, surface temperatures (and thus potentially stability and inversion strength) depend on turbulent and conductive heat fluxes to the surface (Sterk et al, 2013). To examine the extent to which different turbulent or conductive heat fluxes may cause differences in low-level stability, we perturb stable boundary layer diffusivity and snow conductivity in the ECHAM6 SCM and rerun our idealized experiment (Figure 17).

When diffusivity under stably stratified conditions is increased, the cloud deepens faster during the first days and the transition to clear skies happens earlier (not shown). We attribute this change to stronger mixing between the cloud and free-tropospheric air, which is a source of moisture to the Arctic boundary layer (Solomon et al, 2013), leading to faster condensation and hence drying of the atmospheric column. Under clear skies, the turbulent heat flux towards the

surface is reduced by about 25 percent in a run with reduced diffusivity, resulting in slightly stronger stability. Downward turbulent heat fluxes almost double in the increased diffusivity run, leading to a reduction of low-level stability strength by several Kelvin.

The ocean beneath the sea ice is typically 10 to 40 K warmer than the Arctic wintertime atmosphere and thus constitutes a potentially important source of heat. Heat conduction to the atmosphere must be balanced by latent heat release from sea ice formation. How much heat is conducted to the surface depends on the thickness, density and specific conductivities of ice and snow. We here vary the conductivity of snow (shown as stars and triangles in Figure 17) as a proxy for inter-model differences in any of those quantities or in model formulations influencing conductive heat fluxes. Inversion strength in the clear state is almost doubled when snow conductivity is halved and is reduced to less than half the standard value when conductivity is doubled. Despite these impacts on low-level stability, turbulent heat fluxes towards the surface remain almost unchanged.

Sterk et al (2013) studied the impact of both turbulent diffusivity and ice conductivity on surface fluxes and near-surface temperatures in a clear-sky stable boundary layer SCM experiment. They found a stronger sensitivity of fluxes and surface temperatures to turbulent diffusivity under strong winds ($8 ms^{-1}$), while conductive heat flux and clear-sky radiative transfer calculations were more important at low wind speeds ($2 ms^{-1}$). This confirms that both conductive and turbulent heat fluxes may affect low-level stability and temperature inversions under radiatively clear skies, but also shows that different stable boundary-layer regimes should be considered when analyzing what role each processes actually plays in a specific model.

In summary, the overestimation of stable boundary-layer diffusivity in most large-scale models may contribute to the lack of mixed-phase clouds in CMIP5 models. Weak low-level stability under radiatively clear skies as seen in the third group of CMIP5 models can be caused by excessive turbulent mixing or by excessive heat conduction through snow and ice.

6 Conclusions

We have shown that an idealized single-column experiment of the formation of an Arctic air mass driven by radiative cooling and cloud processes can reproduce the observed occurence of a cloudy and a clear state of the Arctic winter boundary layer. The cloudy state characterised by little to no surface longwave cooling occurs when the formation of a liquid or mixed-phase cloud is triggered by radiative cooling of a relatively warm and moist air mass advected into the Arctic from lower latitudes. As the cloud cools, it transforms into a lower emissivity ice cloud that permits stronger surface cooling and is therefore associated with the radiatively clear state of the boundary layer. When the ice cloud has precipitated out, the boundary layer remains in the clear state until a new moist airmass is advected in. During the formation of Arctic air, inversions are formed by advection, eroded by cooling at the cloud level and formed again by surface cooling in the clear state. This results in two typical quasi-stable states, with inversions being stronger in the clear than in the cloudy state.

Changing individual parameterizations in the SCM and comparing results to the standard model, we find that the representation of mixed-phase cloud microphysics is key to successfully modelling the two boundary layer states. Freezing of supercooled water at too warm temperatures that occurs in many CMIP5 models leads to a lack of high-emissivity mixed-phase clouds and thus of a cloudy state in these models. Models lacking a cloudy state display excessive surface radiative cooling in Arctic winter, which tends to produce strong low-level stability and temperature inversions. However, weak temperature inversions in the absence of high-emissivity clouds may be sustained through excessive downward turbulent heat fluxes from the atmosphere or excessive conductive heat fluxes from the ocean, both of which warm the surface.

These processes control the representation of the two boundary layer states and inversion strengths in the CMIP5 models:

1. Few models that allow for cloud liquid water at very low temperatures reproduce both the clear and cloudy state of the boundary layer. Among these models, mean low-level stability depends mostly on the relative occurrence of the two states.
2. A second group of models lacks the cloudy state and exhibits strong stability and strong longwave cooling.
3. Other models also lack the cloudy state, but generate weak stability despite strong longwave cooling. This may be caused by excessive sensible and/or conductive heat fluxes to the surface.

The CMIP5 intermodel spread of typical monthly-mean low-level stability over sea ice in winter is about 10 K, which is similar to that in CMIP3 models (Medeiros et al, 2011). 15 out of 21 CMIP5 models overestimate low-level stability over sea ice compared to reanalyses data, and we argue that this overestimation is substantially larger than biases in the reanalyses. We have shown that this widespread model bias is linked to shortcomings in the representation of mixed-phase cloud microphysics. Models that do exhibit a reasonably frequent cloudy state also exhibit mean low-level stability in good agreement with reanalyses. To understand the causes of biases in turbulent fluxes and/or heat conduction which likely cause weak low-level stability despite strong surface radiative cooling, a closer analysis of the af-

fected third group of models would be necessary. Likewise, the differences in cloud properties, energy fluxes and inversion strengths between land and sea ice domains remain to be investigated.

To advance our understanding of the formation of Arctic air masses and to further link model performance to specific parameterisations, we suggest comparing the results of a wider range of single-column models for an idealised case of warm air advection into the Arctic. In order to better represent the Arctic winter boundary layer and surface energy budget in climate models, an important step would be to improve the mixed-phase cloud microphysics and to obtain an adequate representation of the cloudy state.

Acknowledgements We are grateful to Tiina Kippeläinen for the inspiration to parts of this study, Anthony del Genio for information on the GISS model, Tongwen Wu for information on the BCC-CSM-1-1 model, Suvarchal Kumar Cheedela for developing and helping with the single-column version of ECHAM6 and Bjorn Stevens for helpful comments and discussions. Comments by Dirk Notz helped to improve the clarity of the manuscript. We are grateful to two anonymous reviewers for concise and helpful comments that enabled us to substantially improve the present paper. We thank the investigators involved in the collection and processing of SHEBA and ARM observations for making those datasets available. ERA40 and ERA-interim reanalyses data have been obtained from the ECMWF data server. The HadCRUT3v dataset has been provided by the Climatic Research Unit at the University of East Anglia. We acknowledge the World Climate Research Programme's Working Group on Coupled Modelling, which is responsible for CMIP5, and we thank the climate modeling groups (listed in Table 1) for producing and making available their model output. Plots in this paper have been generated using NCL (UCAR/NCAR/CISL/VETS, 2012) provided by NCAR. Brian Medeiros acknowledges support by the Office of Science (BER), U.S. Department of Energy. NCAR is sponsored by the National Science Foundation.

References

Abbot DS, Tziperman E (2008) A high-latitude convective cloud feedback and equable climates. Q J Roy Met Soc 134(630):165–185, DOI 10.1002/qj.211

ACIA (2004) Impacts of a Warming Arctic-Arctic Climate Impact Assessment. Cambridge University Press

Andreas EL, Guest PS, Persson POG, Fairall CW, Horst TW, Moritz RE, Semmer SR (2002) Near-surface water vapor over polar sea ice is always near ice saturation. Journal of Geophysical Research: Oceans 107(C10):SHE 8–1–SHE 8–15, DOI 10.1029/2000JC000411, URL http://dx.doi.org/10.1029/2000JC000411

Barrett A (2012) Why can't models simulate mixed-phase clouds correctly? PhD thesis, University of Reading

Bergeron T (1935) On the physics of clouds and precipitation. In: Proc. 5th Assembly, UGGI, Lisbon, pp 156–178

Bintanja R, Graversen R, Hazeleger W (2011) Arctic winter warming amplified by the thermal inversion and consequent low infrared cooling to space. Nat Geosci 4:758–761

Cesana G, Kay J, Chepfer H, English J, de Boer G (2012) Ubiquitous low-level liquid-containing Arctic clouds: New observations and climate model constraints from CALIPSO-GOCCP. Geophys Res Letters 39(20):L20,804

Curry J (1983) On the Formation of Continental Polar Air. J Atmos Sci 40:2278–2292

Curry J (1986) Interactions among turbulence, radiation and microphysics in Arctic stratus clouds. J Atmos Sci 43(1):90–106

Cuxart J, Holtslag A, Beare R, Bazile E, Beljaars A, Cheng A, Conangla L, Ek M, Freedman F, Hamdi R, et al (2006) Single-column model intercomparison for a stably stratified atmospheric boundary layer. Boundary-layer Met 118(2):273–303

Devasthale A, Sedlar J, Tjernström M (2011) Characteristics of water-vapour inversions observed over the arctic by atmospheric infrared sounder (airs) and radiosondes. Atmos Chem Phys 11:9813–9823

Donner L, Wyman B, Hemler R, Horowitz L, Ming Y, Zhao M, Golaz J, Ginoux P, Lin S, Schwarzkopf M, et al (2011) The dynamical core, physical parameterizations, and basic simulation characteristics of the atmospheric component AM3 of the GFDL global coupled model CM3. J Climate 24(13):3484–3519

Findeisen W (1938) Die kolloidmeteorologischen Vorgänge bei der Niederschlagsbildung. Meteor Z 55:121–133

Francis JA, Vavrus SJ (2012) Evidence linking arctic amplification to extreme weather in mid-latitudes. Geophysical Research Letters 39(6)

Fridlind AM, Van Diedenhoven B, Ackerman AS, Avramov A, Mrowiec A, Morrison H, Zuidema P, Shupe MD (2012) A fire-ace/sheba case study of mixed-phase arctic boundary layer clouds: entrainment rate limitations on rapid primary ice nucleation processes. Journal of the Atmospheric Sciences 69(1):365–389

Gent P, Danabasoglu G, Donner L, Holland M, Hunke E, Jayne S, Lawrence D, Neale R, Rasch P, Vertenstein M, et al (2011) The community climate system model version 4. J Climate 24(19):4973–4991

Gettelman A, Walden V, Miloshevich L, Roth W, Halter B (2006) Relative humidity over Antarctica from radiosondes, satellites, and a general circulation model. J Geophys Res 111(D9):D09S13

Held I (1978) The Tropospheric Lapse Rate and Climatic Sensitivity: Experiments with a Two-Level Atmospheric Model. J Atmos Sci 35:2083–2098

Honda M, Inoue J, Yamane S (2009) Influence of low arctic sea-ice minima on anomalously cold eurasian winters. Geophysical Research Letters 36(8):L08,707, DOI 10.1029/2008GL037079

Hourdin F, Grandpeix J, Rio C, Bony S, Jam A, Cheruy F, Rochetin N, Fairhead L, Idelkadi A, Musat I, et al (2012) LMDZ5B: the atmospheric component of the IPSL climate model with revisited parameterizations for clouds and convection. Climate Dyn DOI 10.1007/s00382-012-1343-y

Jones P, New M, Parker D, Martin S, Rigor I (1999) Surface air temperature and its changes over the past 150 years. Rev Geophys 37(2):173–199

Jungclaus J, Haak H, Latif M, Mikolajewicz U (2005) Arctic-North Atlantic interactions and multidecadal variability of the meridional overturning circulation. J Climate 18(19):4013–4031

Klein SA, McCoy RB, Morrison H, Ackerman AS, Avramov A, de Boer G, Chen M, Cole JN, Del Genio AD, Falk M, et al (2009) Intercomparison of model simulations of mixed-phase clouds observed during the arm mixed-phase arctic cloud experiment. i: Single-layer cloud. Quarterly Journal of the Royal Meteorological Society 135(641):979–1002

Lohmann U, Roeckner E (1996) Design and performance of a new cloud microphysics scheme developed for the ECHAM general circulation model. Climate Dyn 12(8):557–572

Manabe S, Wetherald R (1975) The effects of doubling the CO2 concentration on the climate of a general circulation model. J Atmos Sci 32:3–15

Mauritsen T, Stevens B, Roeckner E, Crueger T, Esch M, Giorgetta M, Haak H, Jungclaus J, Klocke D, Matei D, et al (2012) Tuning the climate of a global model. J Adv Model Earth Sys 4:M00A01, DOI 10.1029/2012MS000154

Medeiros B, Deser C, Tomas R, Kay J (2011) Arctic inversion strength in climate models. J Climate 24:4733–4740

Météo France (2009) ARPEGE-Climat V5.1 Algorithmic documentation. Tech. rep., Météo France/CNRM

Morrison H, de Boer G, Feingold G, Harrington J, Shupe M, Sulia K (2012) Resilience of persistent Arctic mixed-phase clouds. Nat Geosci 4:11–17, DOI 10.1038/ngeo1332

Overland J, Guest P (1991) The Arctic snow and air temperature budget over sea ice during winter. J Geophys Res 96(C3):4651–4662

Pavelsky T, Boé J, Hall A, Fetzer E (2011) Atmospheric inversion strength over polar oceans in winter regulated by sea ice. Climate Dyn 36(5):945–955

Persson P, Uttal T, Intrieri J, Fairall C, Andreas E, Guest P (1999) Observations of large thermal transitions during the arctic night from a suite of sensors at sheba. In: Third Symposium on Integrated Observing SystemsAm. Meteorol. Soc. Dallas, Tex

Persson P, Fairall C, Andreas E, Guest P, Perovich D (2002) Measurements near the Atmospheric Surface Flux Group tower at SHEBA: Near-surface conditions and surface energy budget. J Geophys Res 107(10.1029)

Pithan F, Mauritsen T (2013) Statistical artifacts in 'Current GCMs' unrealistic negative feedback in the Arctic' by Boé et al. J Climate DOI 10.1175/JCLI-D-12-00331.1

Rotstayn L, Ryan B, Katzfey J (2000) A scheme for calculation of the liquid fraction in mixed-phase stratiform clouds in large-scale models. Monthly weather review 128(4):1070–1088

Schmidt G, Ruedy R, Hansen J, Aleinov I, Bell N, Bauer M, Bauer S, Cairns B, Canuto V, Cheng Y, et al (2006) Present-day atmospheric simulations using GISS ModelE: Comparison to in situ, satellite, and reanalysis data. J Climate 19(2):153–192

Scoccimarro E, Gualdi S, Bellucci A, Sanna A, Giuseppe Fogli P, Manzini E, Vichi M, Oddo P, Navarra A (2011) Effects of Tropical Cyclones on Ocean Heat Transport in a High-Resolution Coupled General Circulation Model. J Climate 24(16):4368–4384

Serreze M, Schnell R, Kahl J (1992) Low-level temperature inversions of the Eurasian Arctic and comparisons with Soviet drifting station data. J Climate 5(6):615–629

Simmons A, Uppala S, Dee D, Kobayashi S (2007) ERA-Interim: New ECMWF reanalysis products from 1989 onwards. ECMWF newsletter 110:25–35

Solomon A, Shupe MD, Persson POG, Morrison H, Yamaguchi T, Feingold G, Caldwell PM, deBoer G (2013) The sensitivity of springtime Arctic mixed-phase stratocumulus clouds to surface layer and cloud-top inversion layer moisture sources. J Atmos Sci submitted

Sorteberg A, Kattsov V, Walsh JE, Pavlova T (2007) The Arctic surface energy budget as simulated with the IPCC AR4 AOGCMs. Climate Dyn 29(2):131–156

Sterk H, Steeneveld G, Holtslag A (2013) The role of snow-surface coupling, radiation, and turbulent mixing in modeling a stable boundary layer over arctic sea ice. Journal of Geophysical Research: Atmospheres 118:1199–1217

Stevens B, Crueger T, Esch M, Giorgetta M, Mauritsen T, Rast S, Schmidt H, Bader J, Block K, Brokopf R, et al (2013) The Atmospheric Component of the MPI-M Earth System Model: ECHAM6. J Adv Model Earth Syst DOI 10.1002/jame.20015

Stramler K, Del Genio A, Rossow W (2011) Synoptically driven Arctic winter states. J Climate 24(6):1747–1762

Svensson G, Karlsson J (2011) On the Arctic Wintertime Climate in Global Climate Models. J Climate 24(22):5757–5771

Sverdrup H (1933) Meteorology, The Norwegian North Polar expedition with the 'Maud' 1918-1925, scientific results, vol II. Geophysical Institute, Bergen, Norway

Taylor K, Stouffer R, Meehl G (2012) An overview of CMIP5 and the experiment design. Bull Am Met Soc 93(4):485

Tjernström M (2012) The Arctic Ocean boundary layer: Interactions with the sea-ice surface and clouds. In: ECMWF GABLS workshop on diurnal cycles and the stable boundary layer, 7-10 November 2011, European Centre for Medium-Range Weather Forecasts

Tjernström M, Graversen R (2009) The vertical structure of the lower Arctic troposphere analysed from observations and the ERA-40 reanalysis. Q J Roy Met Soc 135(639):431–443

Turner JK, Gyakum JR (2011) The Development of Arctic Air Masses in Northwest Canada and Their Behaviour in a Warming Climate. J Climate 24:4818–4633, DOI 10.1175/2011JCLI3855.1

UCAR/NCAR/CISL/VETS (2012) The NCAR Command Language (Version 6.0.0) [Software]. DOI 10.5065/D6WD3XH5

Uppala S, Kållberg P, Simmons A, Andrae U, Bechtold V, Fiorino M, Gibson J, Haseler J, Hernandez A, Kelly G, et al (2005) The ERA-40 re-analysis. Q J Roy Met Soc 131(612):2961–3012

Volodin E, Dianskii N, Gusev A (2010) Simulating present-day climate with the INMCM4.0 coupled model of the atmospheric and oceanic general circulations. Izvestiya Atmospheric and Oceanic Physics 46(4):414–431

Watanabe S, Hajima T, Sudo K, Nagashima T, Takemura T, Okajima H, Nozawa T, Kawase H, Abe M, Yokohata T, et al (2011) MIROC-ESM 2010: model description and basic results of CMIP5-20c3m experiments. Geosci Model Dev 4:845–872

Wegener A (1911) Thermodynamik der Atmosphäre. JA Barth, Leipzig, Germany

Wexler H (1936) Cooling in the lower atmosphere and the structure of polar continental air. Monthly Weather Review 64:122–136

Wu T, Yu R, Zhang F, Wang Z, Dong M, Wang L, Jin X, Chen D, Li L (2010) The Beijing Climate Center atmospheric general circulation model: description and its performance for the present-day climate. Climate Dyn 34(1):123–147

Xie S, McCoy R, Klein S, Cederwall R, Wiscombe W, Jensen M, Johnson K, Clothiaux E, Gaustad K, Long C, et al (2010) CLOUDS AND MORE: ARM Climate Modeling Best Estimate Data. Bull Am Met Soc 91(1):13–20

Yukimoto S, Adachi Y, Hosaka M (2012) A New Global Climate Model of the Meteorological Research Institute: MRI-CGCM3: Model Description and Basic Performance (Special Issue on Recent Development on Climate Models and Future Climate Projections). J Met Soc Japan 90:23–64

Zhang Y, Seidel D, Golaz J, Deser C, Tomas R (2011) Climatological Characteristics of Arctic and Antarctic Surface-Based Inversions. J Climate 24(19):5167–5186